Journal of Superconductivity and Novel Magnetism (2018) 31:2261–2270
https://doi.org/10.1007/s10948-017-4495-5

ORIGINAL PAPER

Ab Initio Theoretical Prediction of Structural, Electronic, and Magnetic Properties in the 3d (Mn)-Doped Zinc-Blende MgSe: A DFT-mBJ Approach

Zeyneb Bordjiba[1] · Athmane Meddour[1] · Chahrazed Bourouis[1]

Received: 29 October 2017 / Accepted: 28 November 2017 / Published online: 8 December 2017

Abstract

In this paper, we have investigated the structural, electronic, and magnetic properties of magnesium selenium (MgSe) doped with transition metal manganese (Mn) impurity in the cubic diluted magnetic semiconductor (DMS) zinc blende structure. The compounds which we are interested are as $Mg_{1-x}Mn_xSe$ where x change between 0 and 1 by step 0.25. All properties are studied, using first-principles calculation of density functional theory under the framework of the full-potential linearized augmented plane waver (FP-LAPW). In our study, we employed the Wu-Cohen generalized approximation (WC-GGA) to optimize the crystal structure, whereas Tran-Blaha modified Becke-Johnson potential (TB-mBJ) as a new functional was applied to compute the electronic and magnetic properties in order to get some better degree of precision. The electronic band structures and density of state plots reveal ferromagnetic semiconducting behavior in these compounds, and the exchange constants $N_0\alpha$ and $N_0\beta$ are calculated to validate the effects resulting from exchange splitting process. Moreover, for each concentration x, the value of total magnetic moment has been estimated to equal to 5 μ_B. The important magnetic moments values obtained in these compounds indicate the potential for their use in spintronic devices.

Keywords MgMnSe · Magnetic properties · TB-mBJ · DMS alloys · Exchange mechanism

1 Introduction

The design and manufacture of new materials with often surprising properties is a very active field of research and modern technology. In this context, semiconductor doped with magnetic impurity represents an important class of materials used in the industry of new technologies; this is because it is possible to control the various physical properties such as the electronic and magnetic properties of the system by adjusting the content of a component of the alloy.

In parallel to this important technological development, spintronic is a new generation of microelectronic, which exploits the spin of charge carriers in the emerging field of promising materials for spin-based multifunctional devices [1–3]. To move forward in this new science, we had to find semiconductor materials having also magnetic properties, which are called diluted magnetic semiconductor (DMS). Where the intensive research of these materials was initiated by the successful doping of non-magnetic semiconductors by magnetic atoms like the 3d transition metal (TM) (Mn, Cr, Ni, Fe, Co, Ti, etc.) or by rare earth metals (RE) (Ho, Gd, Nd, Sm, etc.) [4]. Another important feature of DMSs is that the energy band gap and other physical parameters can be controlled by varying composition of magnetic ions in these materials [5].

The main thrust behind this research is to develop new spintronics devices like spin valves, spin light-emitting diodes, magnetic sensors, logic devices, and ultra-fast optical switches [6].

On the other hand, several experimental [7–13] and theoretical [14–21] research is fixed on the DMSs-based magnetic element doped III–V and II–VI semiconductor to predict their magnetic properties for usages in spintronic application. As well, numerous groups of researchers investigated a large variety of high concentrations of Mn-doped zinc-blende DMS, such as $Mg_{1-x}Mn_xTe$ [22],

✉ Zeyneb Bordjiba
bordjiba.zeyneb@yahoo.com

[1] Laboratoire de Physique des Matériaux, Université 8 Mai 1945 Guelma, BP 401 24000, Guelma, Algeria

$Zn_{1-x}Mn_xS$ [23], $Cd_{1-x}Mn_xTe$ [24], $Be_{1-x}Mn_xSe$, and $Be_{1-x}Mn_xTe$ [25]. It was found that these alloys exhibit a semiconducting nature in both spin channels, making this impurity (Mn) the best choice for finding excellent magnetic property, the reason for which it was used in our theoretical study.

In addition to that, the alkaline earth chalcogenides (AECs) (II = Be, Ca, Sr, Ba; VI = O, S, Se, Te) have engrossed much interest, due to their large band gaps and low dielectrics constants [26–29], making these compounds important for a large variety of optoelectronics devices.

Specifically, magnesium selenium (MgSe) is an attractive binary semiconductor of the II–VI family, which can excite in several phases [30], such as zinc blende with in experimental wide direct band gap of 4 eV at 0 K [31] and lattice constant of 5.89 Å [32]. Used in high-temperature, high-power blue and ultraviolet wavelength optics [32–35] in ZnSe-based laser diodes and light-emitting diodes (LEDs) as a cladding material [35]. Furthermore, some theoretical studies are available in the literature which reported the magnetic properties of MgSe semiconductor doped with 3d TM using the first-principles calculation [36–39].

According to the best of our knowledge, there are no experimental and theoretical studies of structural, electronic, and magnetic properties of Mn-doped MgSe for the full composition range (0–1), which restricts the comparison of our results. In the light of importance of these compounds in various magnetic and optoelectronic applications, our objective in this paper is to investigate the structural, electronic, and magnetic properties of $Mg_{1-x}Mn_xSe$ DMS compounds in the ferromagnetic zinc blende (B3) structure by using the ab initio calculation within the spin-polarization density framework (SP-DFT).

2 Theory and Method of Computation

The calculation of the present study is performed in the formwork of the SP-DFT [40] formulation. We have employed the full-potential linearized augmented plane-wave (FP-LAPW+lo) method [41] as implemented in the WIEN2k code [42] to solve the Kohen-Sham equation [43] in order to investigate physical properties of $Mg_{1-x}Mn_xSe$ ($0 \leq x \leq 1$) compounds in the zinc-blende phase (space group F-43m 216).

However, we consider a standard eight-atom supercell ($Mg_{4-n}Mn_nSe$) which correspond to ($1 \times 1 \times 1$) of zinc-blende phase with cubic symmetry; we obtained the structures of $Mg_{1-x}Mn_xSe$ by replacing the Mg atoms with Mn to get the compounds with 25, 50, and 75% concentrations, respectively.

For $x = 0.25$ and $x = 0.75$, the host lattice exhibit a cubic structure with space group $\bar{4}3m$, while for $x = 0.50$ the crystal present a tetragonal structure with space group $P\bar{4}m2$.

The generalized gradient approximation function developed by Wu and Cohen (WC-GGA) [44] was used as the exchange correlation potential to calculate the ground state parameter, which provides an accurate account of structural properties of solids [45, 46], where for the electronic and magnetic properties the Tran-Blaha modified Becke Johnson (TB-mBJ) [47] approach combined with PBE-GGA are used. It is worth reminding that this approach is not valid for the computations of the equilibrium structural parameters.

As well the combination of TB-mBJ with GGA or local density approximation (LDA) have proved to be relatively better method for computing energy gaps of sp semiconductor, wide band gap semiconductor and transition metalbased materials [47–52].

Also, we are performed using plane wave cutoff of $R_{mt} \times K_{max} = 8$, which control the size of matrix for energy convergence, the R_{mt} is the smallest radii of muffin-tin spheres and K_{max} is the cutoff for the wave function basis. Whereas the Fourier expanded charge density was truncated at $G_{max} = 12$ atomic units $(au)^{-1}$, the values of the atomic radius (muffin-tin RMT) were chosen equal to 2, 2.06, and 2.16 for Mg, Se and Mn respectively in atomic units. The maximum angular momentum quantum number l_{max} is kept at 10 and a k-mesh of $12 \times 12 \times 12$ equivalent to 2000 k points was used for the Brillouin zone (BZ) integration. Finally, the total energy convergence is equal to 10^{-4} Ry when the charge of the system is converged to 0.0001 e.

3 Results and Discussion

3.1 Structural Properties

Firstly, by minimizing the total energy with respect to the volume and fitting it to the empirical Birch-Murnaghan [53] equation of state, the equilibrium lattice constant a and the bulk modulus (B) for $Mg_{1-x}Mn_xSe$ alloys are evaluated in zinc-blende phase (B3) for x vary between 0 and 1 by step of 0.25.

Both MgSe and MnSe have zinc-blend (B3) structure, where Mg and Mn atoms are located at (0, 0, 0) and the Se atom at (1/4, 1/4, 1/4) position. In order to gain deep insight into the physical properties, we have performed volume

Table 1 Calculations of the lattice constant a_0 and the bulk modulus B_0 according to WC-GGA for $Mg_{1-x}Mn_xSe$ alloys after structural optimization

Compound	Lattice constant a_0(Å)			Bulk modulus B_0 (GPa)	
	This work	Cal.	Exp	This work	Cal.
MgSe	5.94	5.93 [38]	5.89 [32]	47.76	48.13 [38]
		5.92 [55]			49.00 [54]
		5.90 [36]			45.86 [36]
$Mg_{0.75}Mn_{0.25}Se$	5.90	–	–	49.72	–
$Mg_{0.50}Mn_{0.50}Se$	5.87	–	–	52.17	–
$Mg_{0.25}Mn_{0.75}Se$	5.86	–	–	55.60	–
MnSe	5.85	5.84 [56]	5.90 [54]	57.86	42.79 [56]
					130.88 [57]

optimization by using the experimental values for binary compounds as of entered parameters.

According to WC-GGA approximation, the calculation of these parameters for binary and ternary compounds in comparison to the experimental and other available theoretical results are presented in Table 1, where the lattice constants of the binary MgSe and MnSe are very close to the experimental values [32, 54] and stay in good agreement with theoretical calculations [36, 38, 55, 56].

Besides, there is some decrease in the lattice constants with increasing Mn concentration for $Mg_{1-x}Mn_xSe$ (x = 0.25, 0.5 and 0.75) because the ionic radius of Mn is smaller compared with Mg atom. While, the compressibility in this alloy increases when the concentration of Mn increase.

We note that there is no experimental and theoretical calculation of lattice constants for $Mg_{1-x}Mn_xSe$ compounds so our results constitute a prediction. As well, the computed lattice constants are used in next calculations of electronic and magnetic properties.

3.2 Electronic Band Structures and Density of States

Most of the physical properties of solids are related to the electronic band structures and the density of states, so the knowledge of these properties is important for its efficient use in optoelectronic, magneto-optic and electromagnetic devices. Here, by using the predicated lattice constant the spin-polarized band structures is computed for $Mg_{1-x}Mn_xSe$ (x = 0.25, 0.50, 0.75 and 1) semiconductor with spin up (↑) and down (↓) orientations along high symmetry of the first BZ in the ferromagnetic zinc blende phase. The curves calculated within TB-mBJ approach to solve the problem of underestimation of band gap are displayed in Figs. 1, 2, 3, 4, and 5. Therefore in the case of $x = 0$ concentration we have treated and plotted the band structure of the binary compound (MgSe) in the non-magnetic (NM) phase (Fig. 1) The Fermi level is set at the zero energy to be considered as a reference point.

From the figures, for both spin orientation (up and down) with $x = 0.25$ to 1 the band structures reveals a direct band gap, where the minimum of the conduction band (CBM) and the maximum of the valence band (VBM) situated at Γ point of the BZ, which possess the semiconducting nature in these alloys.

The direct band gaps of all alloys determined from the spin up case shown in Table 2 are plotted in Fig. 6. For

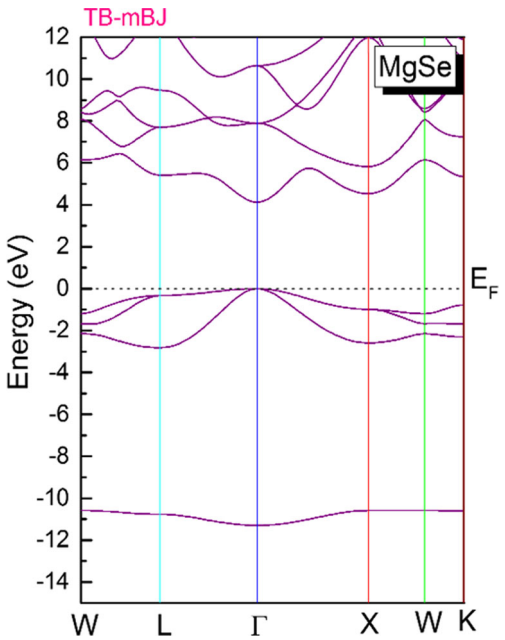

Fig. 1 The band structure of the binary MgSe ($x = 0$) in the non-magnetic phase

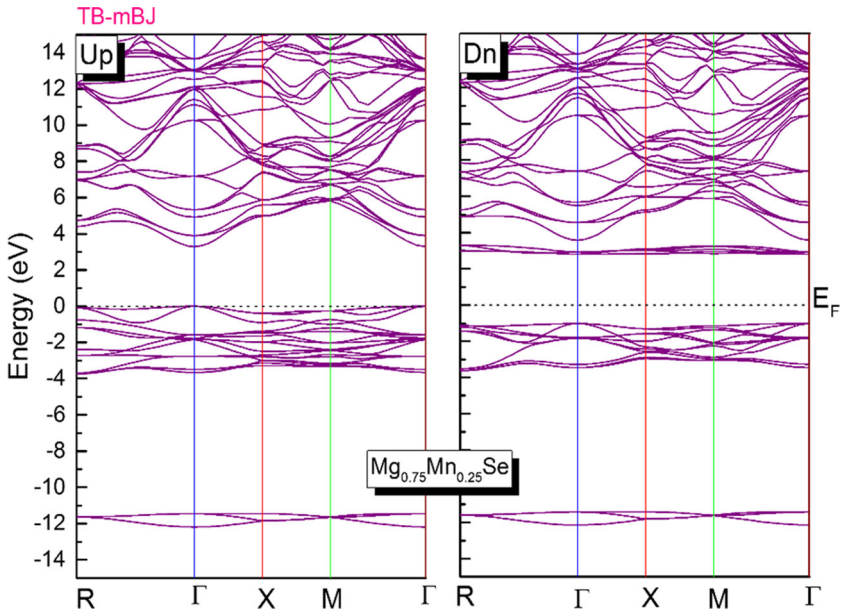

Fig. 2 Spin-polarized band structures of majority spin (up) and minority spin (dn) for $Mg_{0.75}Mn_{0.25}Se$. The Fermi level is set to zero (horizontal dotted line)

further evaluation the band gap energy of $Mg_{1-x}Mn_xSe$ can be depicted as a function of the manganese concentration and expressed by the following formula:

$$E_{g(Mg_{1-x}Mn_xSe)}(x) = xE_{g(MnSe)} + (1-x)E_{g(MgSe)} - x(1-x)b \quad (1)$$

where $E_{g(Mg_{1-x}Mn_xSe)}(x)$ is the band gap energy of the $Mg_{1-x}Mn_xSe$, $E_{g(MgSe)}$ is the band gap energy of the MgSe, $E_{g(MnSe)}$ is the band gap energy of MnSe, and b is the band gap bowing parameter of $Mg_{1-x}Mn_xSe$ alloys.

This equation gives $b = 0.986$ eV, according to the TB-mBJ approximation where the results shown in Fig. 6 was fitted by the expression (1) and follow the quadratic (2)

$$E^{\Gamma-\Gamma}_{g(TB-mBJ)} = 4.094 - 3.281x + 0.986x^2 \quad (2)$$

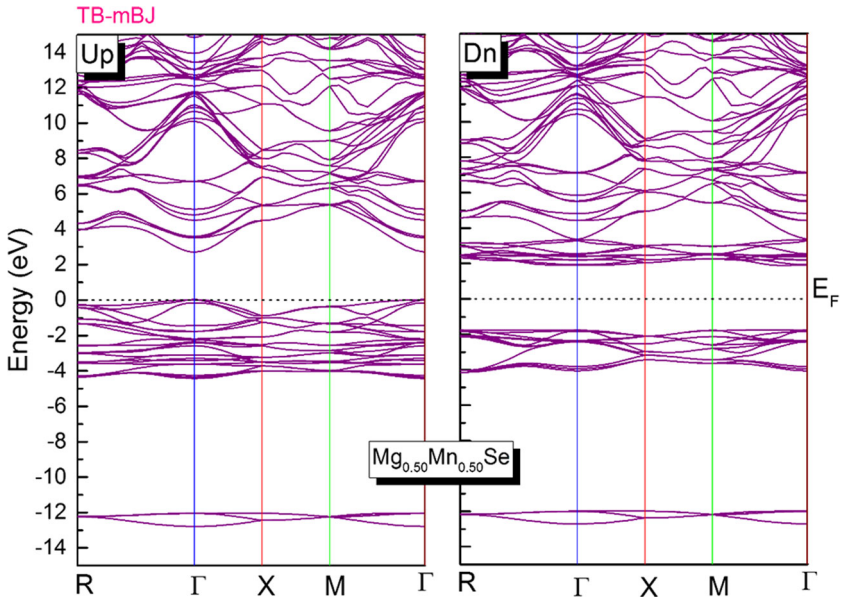

Fig. 3 Spin-polarized band structures of majority spin (up) and minority spin (dn) for $Mg_{0.50}Mn_{0.50}Se$. The Fermi level is set to zero (horizontal dotted line)

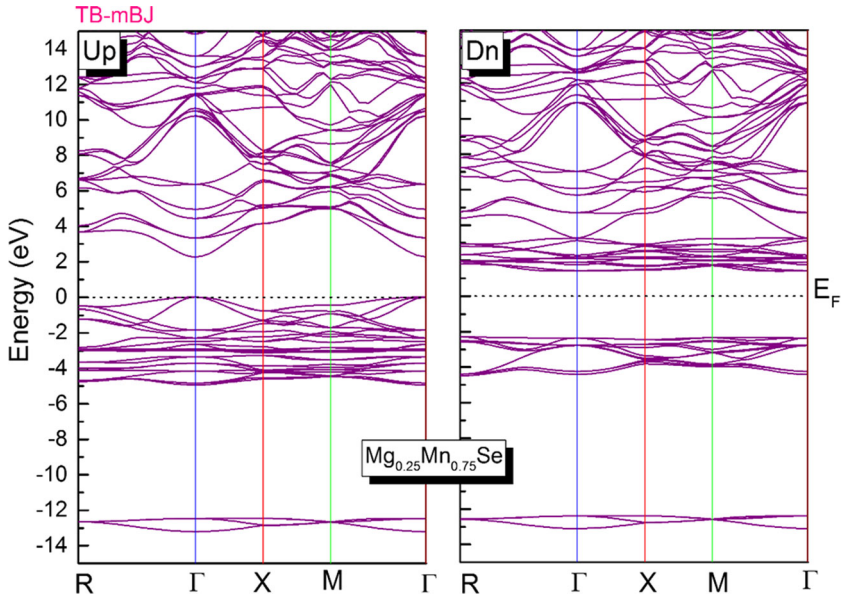

Fig. 4 Spin-polarized band structures of majority spin (up) and minority spin (dn) for $Mg_{0.25}Mn_{0.75}Se$. The Fermi level is set to zero (horizontal dotted line)

As may be seen the energy gap decreases with increased concentration in our compounds. However, in the spin down channels, a symmetric band gap exists around the Fermi level (E_F) for Mn-doped MgSe at all concentrations.

In addition, the different band states of atomic and orbital origins can be explained by calculating the densities of states (DOS) and are displayed in Figs. 7, 8, 9, 10, and 11 for $x = 0$, 0.25, 0.50, 0.75 and 1; the Fermi level E_F is set to zero and it is indicted by the vertical blue dashed line.

According to the crystal field theory, the PDOS curves show that the fivefold degenerate of 3d (Mn) states are divides in two parts: the threefold degenerate high-lying t_{2g} (d_{xy}, d_{yz} and d_{xz}) and the twofold generate low-lying e_g (d_{z^2} and $d_{x^2-y^2}$) symmetry states, this is caused by the effect of the tetrahedral crystal field formed by surrounding (S, Se and Te) ligands; where the energies of e_g states are lower than t_{2g} states due to less Coulomb interaction.

In the case of non-magnetic MgSe ($x = 0$) (Fig. 7), the DOS in the first range from − 11.5 to − 10.5 (eV) is mainly

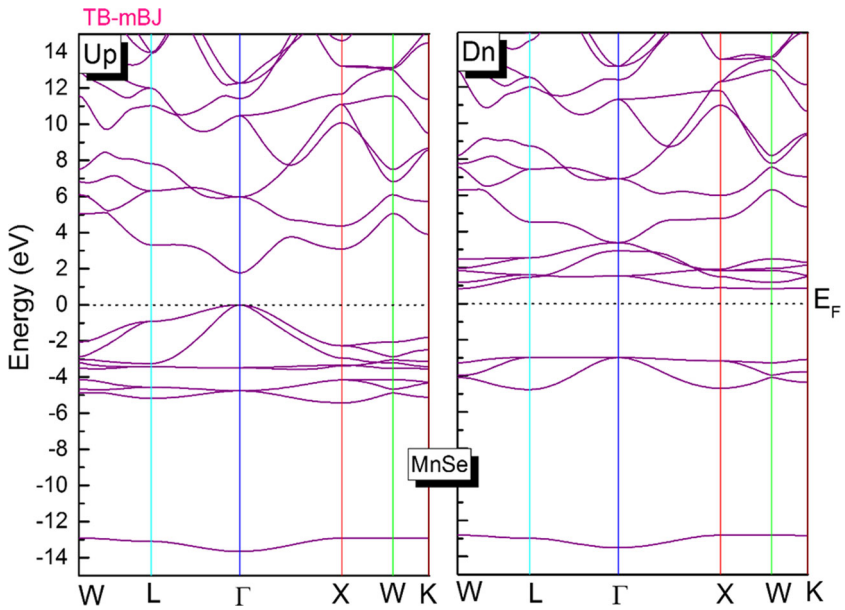

Fig. 5 Spin-polarized band structures of majority spin (up) and minority spin (dn) for MnSe ($x = 1$). The Fermi level is set to zero (horizontal dotted line)

Table 2 The calculated E_g (spin-up band gap), total moments M^{Tot} (μ_B) per Mn, and the local magnetic moments $M^{Mg/Mn/Se}$ for each concentration for $Mg_{1-x}Mn_xSe$ alloys ($x = 0$, 0.25, 0.50, 0.75 and 1) by using TB-mBJ functional

Compound	Band gap (eV)			Magnetic moment (μ_B)			
	$E_g^{\Gamma-\Gamma(Up)}$ Our work	Exp.	Other work	M^{Tot}	M^{Mn}	M^{Mg}	M^{Se}
MgSe	4.12 (NM)	4.00 [31]	4.10 [36] 4.20 [59] 2.60 [36]	–	–	–	–
$Mg_{0.75}Mn_{0.25}Se$	3.290	–	–	5.000	4.383	0.007	0.027
$Mg_{0.50}Mn_{0.50}Se$	2.682	–	–	5.000	4.402	0.015	0.057
$Mg_{0.25}Mn_{0.75}Se$	2.257	–	–	5.000	4.424	0.024	0.075
MnSe	1.767	2.90 [58]	3.65 [57]	5.000	4.489	–	0.100

dominated by "4s" Se orbital. The following range from − 3 (eV) to near the Fermi level (E_F) contain "4p" orbital of Se, while the last region from 4 (eV) to 12 (eV) is dominated by "2p" "3s" Mg and 4p Se orbitals respectively.

For $x = 0.25$, 0.50 and 0.75 (Figs. 8, 9 and 10) we found a great similarity behavior of the density electronic of states. While the lower part range between − 13.5 (eV) and − 11 (eV) is formed by 4sorbitals of Se atom for both spin up-down orientation. As well the DOS in the middle part range around − 5.5 (eV) to near the Fermi level E_F comes essentially from the hybridization between the "3d-e_g" "3d-t_{2g}" Mn and 4p Se, 3s Mg states in the spin up case, conversely the spin down case is dominated by 4p and 4s Se sates. The last one is located between 1.2 (eV) and 15 (eV) and divided into two sub-bands, the first one states from 1.2 (eV) to 5 (eV) formed by 3d-e_g and 3d-t_{2g} Mn states for the spin down case. Where the second one is situated between 5 (eV) and 15 (eV) mainly composed of mixture of 4s, 4p Se and 2p, and 3s Mg orbitals for both spin up and down.

In the case of ferromagnetic MnSe ($x = 1$) (Fig. 11), the DOS in the first range from − 13.6 to − 12.7 (eV) mainly dominated by 4s Se orbital for both spin orientation (up

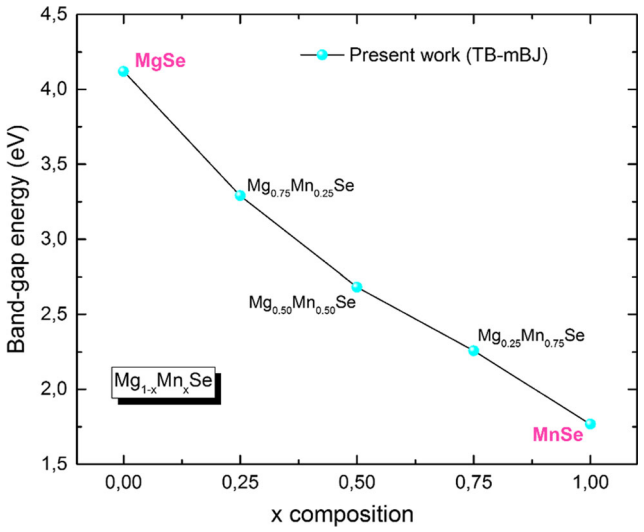

Fig. 6 Band gap as a function of Mn concentrations for $Mg_{1-x}Mn_xSe$

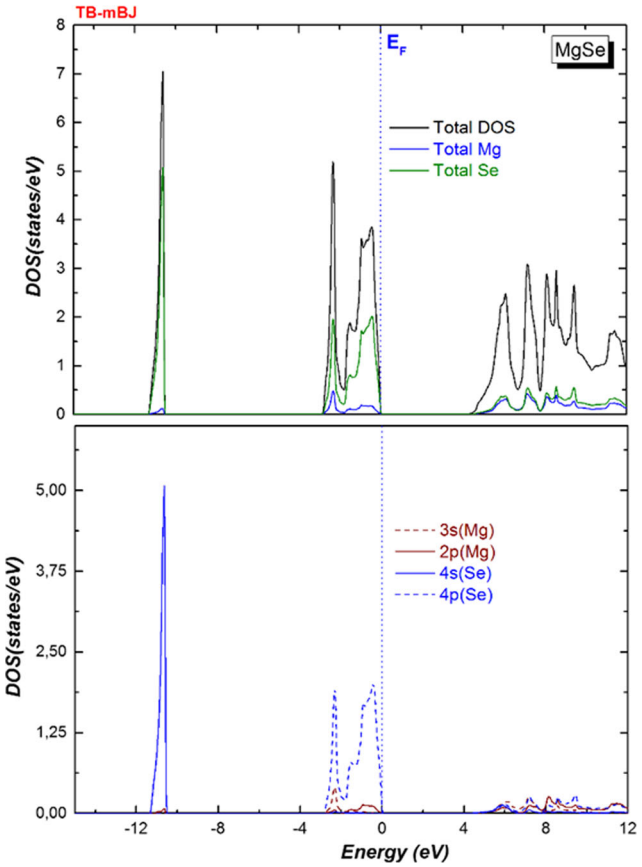

Fig. 7 The total and partial DOS of (2p, 3s) of Mg and (4s, 4p) Se for the binary MgSe ($x = 0$) in the non-magnetic phase. The Fermi level is set to zero (vertical dotted line)

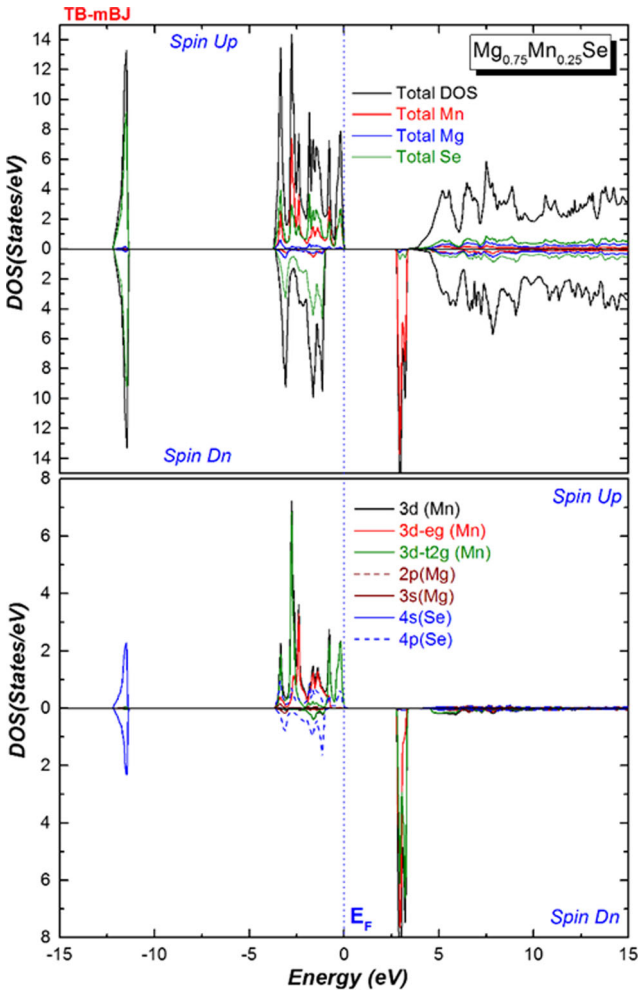

Fig. 8 Spin-polarized total and partial DOS of (2p, 3s) of Mg, (4s, 4p) of Se, and (3d, 3d-t_{2g}, 3d_{eg}) of Mn in supercell of $Mg_{0.75}Mn_{0.25}Se$. The Fermi level is set to zero (vertical dotted line)

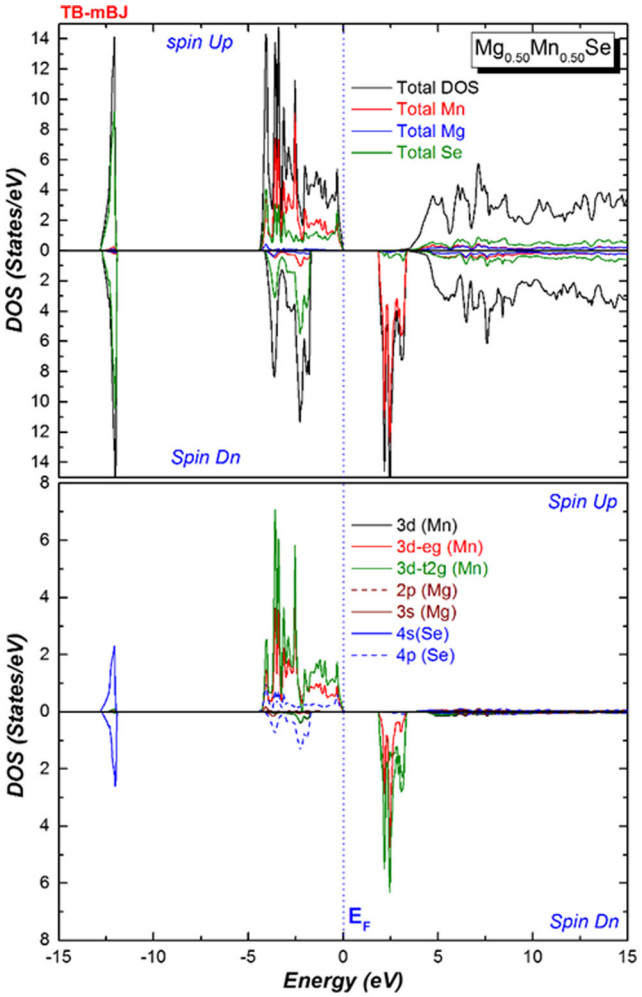

Fig. 9 Spin-polarized total and partial DOS of (2p, 3s) of Mg, (4s, 4p) of Se, and (3d, 3d-t_{2g}, 3d_{eg}) of Mn in supercell of $Mg_{0.50}Mn_{0.50}Se$. The Fermi level is set to zero (vertical dotted line)

and down). The second range from − 5.4 (eV) to near the Fermi level E_F the DOS in the spin up case comes from the hybridization between 3d-e_g, 3d-t_{2g} Mn and 4p Se orbitals, where the spin down case is dominate essentially by the 4p Se orbital. Also, the range between 0.5 (eV) and 5 (eV) is dominated by 3d-e_g and 3d-t_{2g} Mn states for the spin down case, while from 5 to 15 (eV) the region is formed by 4p and 4s Mg orbitals for both spin updown.

On the other side for each concentration, no d-states peak of Mn at the Fermi level for both spin channels (up and down) which exhibit ferromagnetic semiconductor behaviors in these compounds is observed.

3.3 Magnetic Properties and Exchange Coupling

In this section, the values of total and local magnetic moment for DMSs $Mg_{1-x}Mn_xSe$ at different concentrations ($x = 0.25$, 0.5, 0.75 and 1) using TB-mBJ approximation were exerted by first principles calculation are summarized in Table 2.

However, the magnetism in our selected compounds due to 3d (Mn) impurity where the Mn atom contributes two electronic to bonding of host valence band semiconductor resulting in Mn^{+2} ion. As consequence the electronic configuration of 3d (Mn) in our alloys is ($d^5 - e_g^3 t_{2g}^2$) according to the Hund's rule for each concentration. Where all the spin-majority states are occupied but spin-minority states are either empty or partially occupied.

Through Table 2, we observed that local magnetic moment of Mn doped MgSe at $x = 0.25$, 0.50, 0.75 and 1 is reduced less than the predicated Hund's rule values $5\mu_B$ for total magnetic moment due to the p–d exchange interaction. On the other hand, a small contribution of local magnetic moment is induced on the nonmagnetic Mg and Se sites.

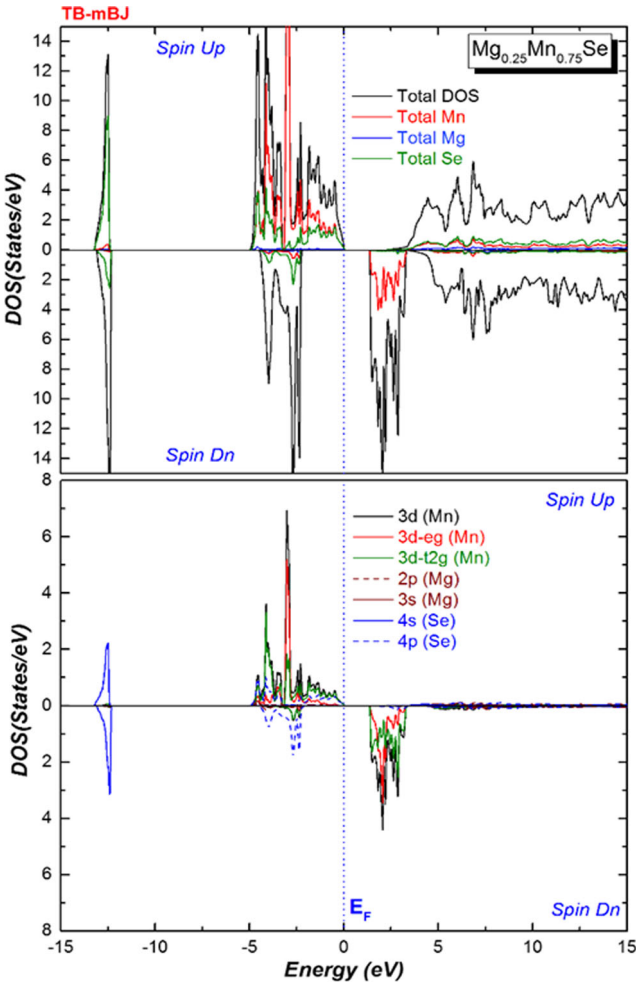

Fig. 10 Spin-polarized total and partial DOS of (2p, 3s) of Mg, (4s, 4p) of Se, and (3d, 3d-t_{2g}, 3d_{eg}) of Mn in supercell of $Mg_{0.25}Mn_{0.75}Se$. The Fermi level is set to zero (vertical dotted line)

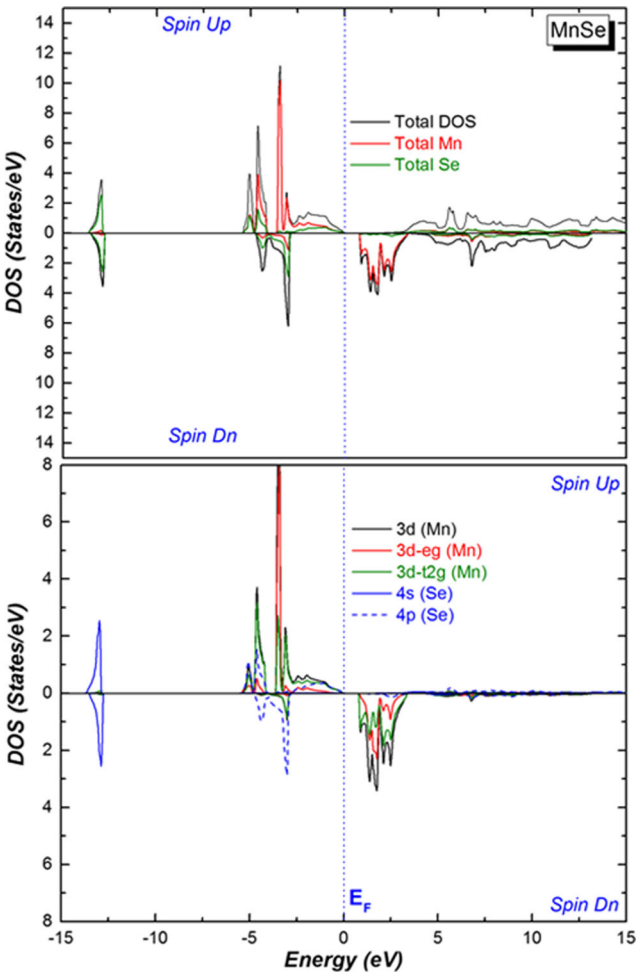

Fig. 11 Spin-polarized total and partial DOS (4s, 4p) of Se, and (3d, 3d-t_{2g}, 3d_{eg}) of Mn for the binary MnSe ($x = 1$). The Fermi level is set to zero (vertical dotted line)

After that, according to the mean field theory, the Hamiltonian given by the following equations [60, 61]:

$$H = -N_0\beta_s.S \tag{3}$$

(where N_0 shows cation content, β expresses p-d exchange, while s and S, respectively, represent free hole and the Mn impurity spins) is employed to find tow important type of exchange constants $N_0\alpha$ and $N_0\beta$ which demonstrate the strength of the s–d and p–d couplings respectively.

As well, the parameters can be calculated from the band structure and the magnetic properties by assuming the usual Kondo interactions [62]:

$$N_0\alpha = \frac{\Delta E_C}{x\langle S\rangle} \tag{4}$$

$$N_0\beta = \frac{\Delta E_V}{x\langle S\rangle} \tag{5}$$

Here, ΔE_C and ΔE_V are band-edge splitting of CBM and VBM respectively, calculated from given equations:

$$\Delta E_C = E^{\downarrow}_{\mathrm{CBMin}} - E^{\uparrow}_{\mathrm{CBMin}} \tag{6}$$

$$\Delta E_V = E^{\downarrow}_{\mathrm{VBMax}} - E^{\uparrow}_{\mathrm{VBMax}} \tag{7}$$

x is the concentration of Mn atom and $\langle S\rangle$ in one half of magnetization per Mn ion. The predicted values of $\Delta E_C \Delta E_V$, $N_0\alpha$ and $N_0\beta$ respectively for each concentration of x are collected in Table 3.

The negative sign of both $N_0\beta$ and $N_0\alpha$ confirms the double-exchange mechanism in our compounds where the s–d and p–d interactions are parallel and support FM character. In addition, we find that $N_0\beta$ is more negative than $N_0\alpha$ this indicated that the exchange energy involved through the spin-down channel.

Table 3 Calculated conduction ΔE_C and valence ΔE_V band-edge spin-splitting and exchange constants $N_0\alpha$, $N_0\beta$, for $Mg_{1-x}Mn_xSe$ at $x = 0.25$, 0.50, 0.75 and 1 using TB-mBJ functional

Compound	ΔE_C	ΔE_V	$N_0\alpha$	$N_0\beta$
$Mg_{0.75}Mn_{0.25}Se$	− 0.488	− 1.030	− 0.781	− 1.648
$Mg_{0.50}Mn_{0.50}Se$	− 0.791	− 1.771	− 0.632	− 1.417
$Mg_{0.25}Mn_{0.75}Se$	− 0.829	− 2.360	− 0.442	− 1.258
MnSe	− 0.228	− 2.986	− 0.091	− 1.194

4 Conclusion

In this article, we summarize theoretical prediction of the structural, electronic, and magnetic properties of Mn doped MgSe at ($x = 0$, 0.25, 0.50, 0.75 and 1) by using the firstprinciples calculation based on the full potential linear augmented plan wave (FP-LAPW+lo) under the framework of SP-DFT (spin polarization density). Based on our results, the following main conclusion is drawn.

Our results of structure properties are reported for the first time, where the equilibrium lattice constant of $Mg_{1-x}Mn_xSe$ compounds decrease with the addition of Mn dopant.

For the electronic properties, our compounds maintain a semiconducting nature in both spin configuration (up and down) and have a direct band gap.

The calculated total magnetic moments for $Mg_{1-x}Mn_xSe$ are about 5 μ_B largely arisen from the manganese doping; also, we can see a small magnetic moment produce on non-magnetic Mg and Se atom, due to the hybridizations between p (Se) and d (Mn) states.

References

1. Ohno, H.: Science. **281**, 951 (1998)
2. Wolf, S.A., Awschalom, D.D., Buhrman, R.A., Daughton, J.M., von Molnar, S., Roukes, M.L., Chtchelkanova, A.Y., Treger D.M.: Science **294**, 1488 (2001)
3. Zutic', I., Fabian, J., Das Sarma, S.: Rev. Mod. Phys. **76**, 323 (2004)
4. Sato, K., Bergqvist, L., Kudrnovsky, J., Dederichs, P.H., Eriksson, O., Turek, I., Sanyal, B., Bouzerar, G., Katayama-Yoshida, H., Dinh, V.A., Fukushima, T., Kizaki, H., Zeller, R.: Rev. Mod. Phys. **82**, 1633 (2010)
5. Dwarakanadha Reddy, Y., Reddy, B.K., Sreekantha Reddy, D., Reddy, D.R., Spectrochim, J.: Acta Part A **70**, 934 (2008)
6. Saeed, Y., Nazir, S., Shaukat, A., Reshak, A.H.: J. Magn. Magn. Mater. **322**, 3214 (2010)
7. Singh, J., Kumar, S., Verma, N.K.: Mater. Sci. Semicond. Process. **26**, 1 (2014)
8. Torquato, R.A., Shirsath, S.E., Kiminami, R.H.G.A., Costa, A.C.F.M.: Ceram. Int. **40**, 6553 (2014)
9. Tomakin, M., Öncel, Y., Keskenler, E.F., Nevruzoğlu, V., Onuk, Z., Görür, O.: J. Alloys Compd. **616**, 166 (2014)
10. Reddy, D.A., Kim, D.H., Rhee, S.J., Jung, C.U., Lee, B.W., Liu, C.: J. Alloys Compd. **588**, 596 (2014)
11. Fang, W., Liu, Y., Guo, B., Peng, L., Zhong, Y., Zhang, J., Zhao, Z.: J. Alloys Compd. **584**, 240 (2014)
12. Silva, A.S., Franco, A., Pelegrini, F., Dantas, N.O.: J. Alloys Compd. **647**, 637 (2015)
13. Akhtar, M.S., Malik, M.A., Alghamdi, Y.G., Ahmad, K.S., Riaz, S., Naseem, S.: Mater. Sci. Semicond. Process. **39**, 283 (2015)
14. Bourouis, C.h., Meddour, A.: J. Magn. Magn. Mater. **324**, 1040 (2012)
15. Gous, M.H., Meddour A., Bourouis Ch.: J. Supercond. Nov. Magn. (2016)
16. Gous, M.H., Meddour, A., Bourouis, C.h.: J. Magn. Magn. Mater. **422**, 271 (2017)
17. Yahi, H., Meddour, A.: J. Magn. Magn. Mater. **401**, 116 (2016)
18. Yahi, H., Meddour, A.: J. Magn. Magn. Mater. **432**, 591 (2017)
19. Doumi, B., Mokaddem, A., Temimi, L., Beldjoudi, N., Elkeurti, M., Dahmane, F., Sayede, A., Tadjer, A., Ishak-Boushaki, M.: Eur. Phys. J. B. **88**, 1 (2015)
20. Doumi, B., Mokaddem, A., Dahmane, F., Sayede, A., Tadjer, A.: RSC Adv. 5 (2015)
21. Mahmood, Q., Alay-e-Abbas, S.M., Mahmood, I., Asif, M., Noor, N.A.: Chinese Phys. B. **25**, 47101 (2016)
22. Noor, N.A., Ali, S., Tahir, W., Shaukat, A., Reshak, A.H.: J. Alloys Compd. **509**, 8137 (2011)
23. Hassan, M., Noor, N.A., Mahmood, Q., Amin, B.: Curr. Appl. Phys. **16**, 1473 (2016)
24. Gueddim, A., Madjet, M.E., Zerroug, S., Bouarissa, N.: Opt. Quantum Electron. **48**, 551 (2016)
25. Noor, N.A., Alay-e-Abbas, S.M., Saeed, Y., Ghulam Abbas, S.M., Shaukat, A.: J. Magn. Magn. Mater. **339**, 11 (2013)
26. Saib, S., Bouarissa, N., Rodriguez-Hernndez, P., Munoz, A.: Eur. Phys. J. B **73**, 185 (2010)
27. Pandey, R., Sivaraman, S.: J. Phys. Chem. Solids **52**, 211 (1991)
28. Rached, D., Benkhettou, N., Soudini, B., Abbar, B., Sekkal, N., Driz, M.: Phys. Stat Sol. (b) **240**, 565 (2003)
29. Wang, M.W., Phillips, M., Swenberg, J.F., Yu, E.T., McCaldin, J.O., McGill, T.C.: J. Appl. Phys. **73**, 4660 (1993)
30. Mir, S.H., Jha, P.C., Dabhi, S., Jha, P.K.: Mater. Chem. Phys. (2016)
31. Jobst, B., Hommel, D., Lunz, U.: Appl. Phys. **69**, 97 (1996)
32. Okuyama, H., Nakano, K., Miyajima, T., Akimato, K.: J. Cryst. Growth **117**, 139 (1992)
33. ThLitz, M., Watanabe, K., Korn, M., Ress, H., Lunz, U., Ossau, W., Waag, A., Landwehr, G., Walter, T.h., Neubauer, B., Gerthsen, D., Schussler, U.: J. Cryst. Growth **159**, 54 (1996)
34. Duman, S., Bagci, S., Tutuncu, H.M., Srivastava, G.P.: Phys. Rev. B **73**, 205201 (2006)
35. Elsayed, H., Olgun, D., Cantarero, A., Hernandez-Calderon, I.: Phys. Status Solidi B **252**(No. 4), 663 (2015)
36. Noor, N.A., Alay-E-Abbas, S.M., Sohaib, M.U., Ghulam Abbas, S.M., Shaukat, A.: J. Magn. Magn. Mater. **374**, 164 (2015)
37. Rashid, M., Ahmad, S.A., Abo, G.S., Imran, M., Hussain, F., Noor, N.A., Karim, A.: Mater. Sci. Semicond. Process. **33**, 110 (2015)
38. Sajjad, M., Zhang, H.X., Noor, N.A., Alay-e-Abbas, S.M., Younas, M., Abid, M., Shaukat, A.: J. Supercond. Nov. Magn. **27**, 2327 (2014)

39. Mahmood, Q., Alay-e-Abbas, S.M., Yaseen, M., Mahmood, A., Rashid, M., Noor, N.A.: J. Supercond. Nov. Magn (2016)
40. Hohenberg, P., Kohn, W.: Phys. Rev. B **136**, 864 (1964)
41. Koelling, D.D., Harmon, B.N.: J. Phys. C: Solid State Phys. **10**, 3107 (1977)
42. Blaha, P., Schwarz, K., Madsen, G.K.H., Kvasnicka, D., Luitz, J.: WIEN2K, an augmented plane wave + local orbitals program for calculating crystal properties karlheinz Schwarz, Techn. Wien, Austria (2014)
43. Kohn, W., Sham, L.: J. Phys. Rev. A **140**, 1133 (1965)
44. Wu, Z., Cohen, R.E.: Phys. Rev. B **73**, 235116 (2006)
45. Wong, K.M., Alay-e-Abbas, S.M., Fang, Y., Shaukat, A., Lie, Y.: J. Appl. Phys. **114**, 034901 (2013)
46. Alay-e-Abbas, S.M., Nazir, S., Mun Wong, K., Shaukat, A., Schwingenschlögl, U.: EPL Europhysics Lett. **106**, 27003 (2014)
47. Tran, F., Blaha, P.: Phys. Rev. Lett. **102**, 226401 (2009)
48. Jiang, H.: J. Chem. Phys. **138**, 134115 (2013)
49. Ali, R., Mohammad, S., Ullah, H., Khan, S.A., Uddin, H., Khan, M., Khan, N.U.: Phys. B Condens. Matter. **410**, 93 (2013)
50. Iqbal, R., Khan, I., Rahnamaye Aliabad, H.A., Ali, Z., Ahmad, I.: J. Magn. Magn. Mater. **351**, 60 (2014)
51. Mahmood, Q., Hassan, M., Faridi, M.A.: Chinese Phys. B. **26**, 27503 (2017)
52. Mahmood, Q., Hassan, M., Noor, N.A.: J. Phys. Condens. Matter. **28**, 506001 (2016)
53. Birch, F.: Phys. Rev. **71**, 809 (1947)
54. Furdyna, J.K.: J. Applied Physics **64**, R29 (1988)
55. Duman, S., Bagcı, S., Tütüncü, H.M., Srivastava, G.P.: Phys. Rev. B **73**, 205201 (2006)
56. Noor, N.A., Alay-e-Abbas, S.M., Saeed, Y., Ghulam Abbas, S.M., Shaukat, A.: J. Magn. Magn. Mater. **339**, 11 (2013)
57. Benkhettou, N., Bensaid, D.: Condens. Matter Phys. 29 (2008)
58. Imamura, M., Okada, A.: IEEE Trans. Magn. **42**(10), 3078 (2006)
59. Ali, R., Mohammad, S., Ullah, H., Khan, S.A., Uddin, H., Khan, M., Khan, N.U.: Phys. B Condens. Matter. **410**, 93 (2013)
60. Huang, Y., Jie, W., Zha, G.: J. Alloys Compd. **555**, 117 (2013)
61. Gaj, G.A., Planel, R., Fishman, G.: Solid State Commne. **29**, 435 (1979)
62. Sanvito, S., Ordejon, P., Hill, N.A.: Phys. Rev. B **63**, 165206 (2001)